

MimicTouch: Learning Human’s Control Strategy with Multi-Modal Tactile Feedback

Kelin Yu¹, Yunhai Han¹, Matthew Zhu¹, Ye Zhao¹

¹Georgia Institute of Technology
(kyu85, yhan389, matthewjzhu0520, yezhao)@gatech.edu

Abstract: In robotics and artificial intelligence, the integration of tactile processing is becoming increasingly pivotal, especially in learning to execute intricate tasks like alignment and insertion. However, existing works focusing on tactile methods for insertion tasks predominantly rely on robot teleoperation data and reinforcement learning, which do not utilize the rich insights provided by human’s control strategy guided by tactile feedback. For utilizing human sensations, methodologies related to learning from humans predominantly leverage visual feedback, often overlooking the invaluable tactile feedback that humans inherently employ to finish complex manipulations. Addressing this gap, we introduce “MimicTouch”, a novel framework that mimics human’s tactile-guided control strategy. In this framework, we initially collect multi-modal tactile datasets from human demonstrators, incorporating human tactile-guided control strategies for task completion. The subsequent step involves instructing robots through imitation learning using multi-modal sensor data and retargeted human motions. To further mitigate the embodiment gap between humans and robots, we employ online residual reinforcement learning on the physical robot. Through comprehensive experiments, we validate the safety of MimicTouch in transferring a latent policy learned through imitation learning from human to robot. This ongoing work will pave the way for a broader spectrum of tactile-guided robotic applications.

1 Introduction

In the field of robotics and automation, performing intricate tasks like insertion remains a formidable challenge. The primary reasons are the dynamic interactions among objects influenced by various factors, including material properties, surface textures, and minor misalignment. As a result, a minor execution error might result in catastrophic task failure. This underscores the need for adaptive insertion mechanisms with real-time feedback. To tackle this problem, many methods, including recent advancements by NVIDIA, have leaned heavily on vision-based solutions [1, 2, 3, 4]. Their “IndustReal” system [1] adeptly transfers assembly tasks learned in simulations to real-world applications, and it achieves a remarkable success rate of up to 99.2% using a customized simulator, “Factory” [2], for modeling the contact-rich interactions. However, these approaches primarily rely on visual feedback, which might fall short in environments where visual feedback is compromised by the occlusions or varying lighting conditions.

In contrast, humans exhibit innate fine-grained manipulation skills through tactile sensing, allowing for successful insertions by solely using tactile sensations to assess alignment, pose, and force, even without visual input [5]. This ability underscores the wealth of information that tactile feedback offers. Motivated by this, several recent studies have delved into the potential of tactile feedback for complex contact-rich tasks. One approach combined visual, auditory, and tactile perception to enhance robots’ capabilities for complex manipulation tasks [6, 7, 8]. Another study proposed to learn a tactile-based feedback insertion policy, modeling the insertion as a policy iterating between attempts and pose corrections, primarily through reinforcement learning (RL) [9, 10, 11, 12]. While these studies recognize the significance of tactile feedback, they predominantly rely on robot teleoperation [8, 13, 14] data guided by human visual feedback or RL, which might not utilize human’s tactile-guided control strategy. Therefore, it is imperative to investigate methods that can more authentically incorporate human’s tactile-guided control strategy in robotic systems.

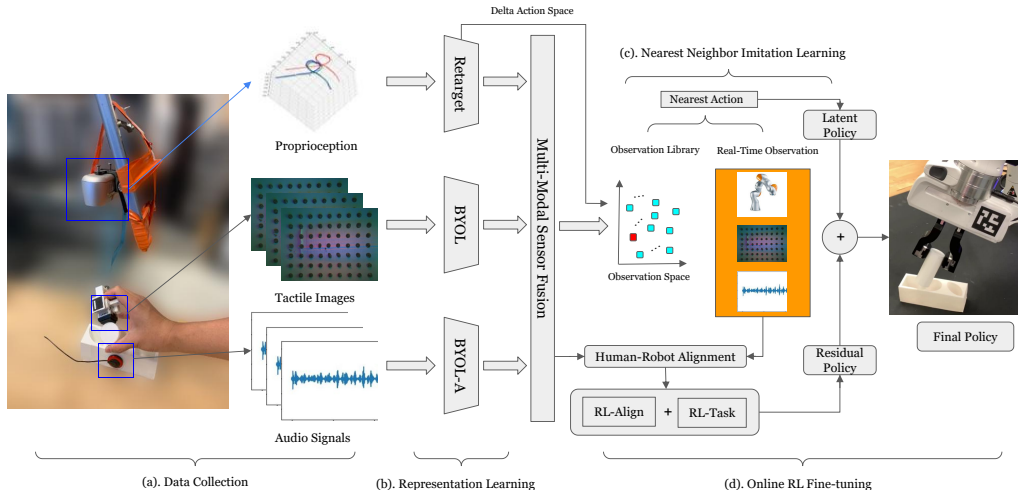


Figure 1: Illustration of our MimicTouch Framework. In part (a), the multi-modal (tactile + audio) tactile feedback is collected during human demonstrations. In part (b), their representation will be learned. In part (c), a latent policy will be learned by Imitation Learning. In part (d), the latent policy will be refined through online residual reinforcement learning on a physical robot.

Learning from human demonstrations has been a long-standing research topic. One particular challenge comes from the embodiment gap, which refers to the differences in sensory and motor capabilities due to the morphology disparity between humans and robots. Recent advancements have primarily focused on leveraging visual feedback and human demonstrations, with two main methodologies emerging. The first utilizes hybrid datasets, combining human and robot teleoperation data to address the embodiment gap and reduce data collection time [15, 16]. The second involves reinforcement learning (RL) fine-tuning [17, 18, 19, 20], to refine pre-trained models to bridge the embodiment gap. While these show significant strides in leveraging visual demonstrations, the human tactile modality remains relatively uncharted. Furthermore, learning human’s tactile-guided control strategy presents distinct challenges, especially given the fact that the embodiment gap and the safety transferring issue are pronounced in the tactile domain. Given the potential benefits of utilizing human’s control strategy guided by tactile feedback, there is a great motivation to solve those challenges and delve deeper into how robots can harness human’s tactile-guided control strategy.

In this work, we present “MimicTouch” (shown in Fig. 1), a novel framework that capitalizes on multi-modal tactile feedback derived from human demonstrations to learn human’s tactile-guided control strategy. The key components of the MimicTouch framework include: 1). A sophisticated human-centric data collection system, designed to collect multi-modal tactile feedback (tactile + audio) to learn human’s tactile-guided control strategy, 2). A representation learning model, adept at extracting task-specific features from diverse inputs, intended to improve the following imitation learning efficiency, 3). A non-parametric imitation learning to learn a latent policy from human demonstrations, which can then be safely transferred into a physical robot, 4). A verification tool to execute the latent policy in the simulator to ensure the safety of subsequent real-world RL fine-tuning. 5). An online residual reinforcement learning method learns a residual policy for fine-tuning the latent policy on a physical robot, which further bridges the embodiment gap between humans and robots and empowers the robot to execute insertion tasks in a manner reminiscent of human expertise. This is our ongoing work, and we hope to show more complete results soon.

Unlike previous methods using teleoperation to collect tactile data, MimicTouch highlights the human’s tactile-guided control strategy. Our approach allows humans to complete contact-rich tasks and generate real-time tactile datasets for robots. Additionally, the ablation study demonstrates enhanced learning efficiency by integrating multi-modal tactile feedback with self-supervised learning models. Finally, by employing latent policy evaluation, we show deployable policy transfer to the

physical robot. In future work, we will fine-tune our latent policy using online RL and conduct extensive experiments in two intricate insertion tasks.

2 Related Works

In this section, we contextualize our contributions within relevant sub-fields.

2.1 Multi-Modal Tactile Sensing

Vision-based tactile sensing is integral to robotic manipulation, with sensors equipped with internal cameras offering high-resolution data on local contact geometry and frictional properties [21, 22, 23, 24]. Through the application of tactile sensing, several learning-based methodologies have been developed for a range of manipulation tasks.

Various studies have incorporated imitation learning algorithms with tactile sensing in multi-modal perception to accomplish intricate tasks such as insertion, dense packing, pouring, and other dexterous manipulation tasks [6, 7, 8]. On the other hand, some researches have focused on employing tactile feedback solely as the reward function of reinforcement learning, successfully completing tasks like insertion, in-hand rotation, and multi-material object cutting without visual feedback [9, 10, 11]. Out of learning-based methodologies, tactile sensing is also widely used in shape reconstruction [25, 26, 27], grasping [28, 29, 30, 31], and dense packing [24]. Nonetheless, the vision-based tactile sensor may not fully represent the features of tactile sensing.

Audio-based tactile sensors, e.g. contact microphones, have been demonstrated to be another effective modality in robotics, such as robot manipulation [32], classifying object instances [33, 34], modeling dynamics [35, 36], and learning food embeddings [37]. Such data can emulate nerve endings within human skin that detect vibrations during tactile interactions, enhancing human’s perception of surface roughness. Furthermore, it facilitates the detection of collisions and slippages between objects [36]. Incorporating this into multi-modal tactile sensing can yield tactile feedback more akin to human sensations, which is helpful for learning human’s tactile-guided control strategy.

2.2 Learning from Human Demonstration

Leveraging human demonstration offers an avenue to leverage human’s tactile-guided control strategy. The domain of learning from human demonstrations, especially from videos [38], has been extensively researched. Given the ease of collecting human demonstrations, the learning process is considerably less time-intensive and more diverse compared to learning from teleoperation data and pure reinforcement learning.

Two prominent methods include hybrid learning from both human and robot teleoperation [15, 16] and model fine-tuning using reinforcement learning [12, 17, 18, 19, 20]. Both methods effectively address the embodiment gap challenges when transitioning from human to robot. In this study, we focus on leveraging genuine human’s tactile-guided control strategy, eschewing robot teleoperation data, and opting for reinforcement learning-based fine-tuning.

2.3 Imitation Learning

For the purpose of our study, it is imperative to employ an imitation learning algorithm to derive a latent policy from human demonstrations. Imitation learning can be bifurcated into two categories: parametric [39, 40, 41] and non-parametric imitation learning [42, 43, 44]. Parametric imitation learning algorithms, which rely on computing a multitude of related parameters, offer superior generalizability. However, they are also prone to a higher covariance shift, making them potentially hazardous when applied directly to out-of-domain executions. In contrast, non-parametric imitation learning algorithms derive insights solely from the observations and trajectories in the dataset, devoid of any additional parameters. While they may be short of generalizability, they offer a safer alternative to their parametric counterparts. Considering our objective of safely learning human’s tactile-guided strategy, we have opted for the non-parametric VINN algorithm [44].

3 Methodology

MimicTouch operates through three distinct phases: 1). Representation learning from task-specific human interactions (see Sec. 3.2), 2). Non-parametric imitation learning with demonstrations from human’s tactile-guided control strategy (see Sec. 3.3), and 3). Online residual reinforcement learning refinement (see Sec. 3.5). Initially, we use our human data collection system (see Sec. 3.1) to gather a specialized multi-modal tactile dataset during insertion tasks. Then, we apply two self-supervised learning models to this dataset, producing optimized representation encoders for both tactile and audio data. During the next phase, we leverage imitation learning with multi-modal tactile feedback sourced from our data collection system, aiming to derive a latent policy. Further, we evaluate the safety of this latent policy in a simulated environment (see Sec. 3.4). The final phase involves the fine-tuning of this latent policy through online residual reinforcement learning. The diagram of this framework is shown in Fig. 1

3.1 Data Collection System

We design a human-centric data collection system (part (a) in Fig. 1), which simultaneously collects the pose of human fingertips, tactile images, and audio signals when humans use their tactile feedback to complete insertion tasks.

Hardware Setting Our data collection system is equipped with specialized hardware for data capture (shown in Fig. 1). The data encompasses three elements: human fingertip pose, which will be retargeted to the pose of the robot end-effector; tactile images, which indicate object-sensor contact; and audio signals, which mimic the vibrations detected by deep skin nerve endings. We use the RealSense camera for fingertip pose tracking, offering a 60 Hz stream at a 320x240-pixel resolution. The GelSight Mini [45], a compact vision-based tactile sensor, facilitates tactile imaging with a 30 Hz stream at 400x300 pixels. This sensor is conveniently mounted onto human fingertips using a custom fixture (refer to Fig. 1). Audio data is captured using the HOYUJI TD-11 piezoelectric contact microphone with a 44.1kHz sampling rate. Due to the fact that robot’s inherent noise differs from that of humans, the microphone is placed at the base of our insertion task (shown in Fig. 1) instead of the end-effector or human fingertips, ensuring consistent audio data collection. For our insertion tasks in Sec. 4.1, the vibration from collisions and slippery will be only helpful to robot policy during the final insertion process when physical contact happens but not during the previous contact-free process. Hence, installing it on the base represents a part of multi-modal tactile sensing and helps learn human’s tactile-guided control strategy.

The details about fingertip pose collections are shown in Appendix. A

3.2 Pre-training Tactile Representation

Representation Learning is the first phase of our framework (part (b) in Fig. 1).

Data Collection For self-supervised learning (SSL) training, we collect task-specific tactile-audio data obtained from human’s tactile-guided insertion tasks shown in Sec. 4.1. Our dataset encompasses success, failed, and sub-optimal instances. Each task yields tactile images at 30 Hz and audio data sampled at 44.1kHz, segmented at 2Hz. In total, we collected 9,157 tactile images and 1,000 audio segments for SSL training.

Representation Learning To extract low-dimensional useful representations from the demonstration data, we employ SSL, which tries to learn a low-dimensional representation from high-dimensional observations. Specifically, we employ the Bootstrap Your Own Latent (BYOL) [46] for tactile images and BYOL for audio (BYOL-A) for audio data [47], which have demonstrated enhanced performance in computer vision [46], audio representation [47], and robotics [8, 13, 32] domains. Details about BYOL and BYOL-A are shown in Appendix. B.

Leveraging BYOL and BYOL-A, we generate two 1×2048 representation vectors for each tactile image and audio segment. Details are shown in Appendix. B

3.3 Learning Latent Policy from Human Demonstration

To learn a latent policy from human demonstration, we use a non-parametric imitation learning algorithm to ensure the safety of policy transferring from human to robot. (part (c) in Fig. 1)

3.3.1 Data Processing

To use data from the human demonstration in physical robots, we need to first integrate data processing.

Data Alignment To ensure synchronization across our sensors, we address the disparate sampling rates of the RealSense, tactile sensor, and audio sensor, which are 60Hz, 30Hz, and 2Hz, respectively. Given the continuous nature of the insertion tasks, a 2Hz sampling rate is insufficient. We downsample the pose and tactile image data to 5Hz. For audio, rather than collecting discrete 0.5s segments, we only capture extended audio data for every 0.2s, resulting in a 0.3s overlap between every two neighboring audio segments. Finally, we obtain one human fingertip pose, one tactile image, and one 0.5s audio segment at 5Hz.

Pose retargeting The 6D human fingertip poses that are extracted from the Aruco marker encompass 3D positions along with rotation vectors. Then, we transform these rotation vectors into Euler angles. The transformed poses function as desired robot end-effector poses. After pose retargeting, we still need post-processing to generate a smooth trajectory. Details are shown in Appendix. C. Finally, the smoothed robot end-effector trajectories are used for further imitation learning.

3.3.2 Non-Parametric Imitation Learning

Our action space is defined by the 6D delta pose transformation of the robot end-effector, encompassing a delta position and a delta Euler angle. Given the inherent challenges of ensuring safety during the transition from human to robot, coupled with the complexity of high-dimensional action and observation spaces, traditional parametric methods often face challenges. These challenges arise from issues such as covariance shifts and the intricacies of learning effective policies in scenarios with limited data. To address these challenges, we employ the nearest neighbors-based imitation learning algorithm (VINN) [44], capitalizing on our collected demonstrations. The observations and actions in the collected demonstrations are shown as $(o_i^T, o_i^A, o_i^e, a_i)$ at the i -th step, where the o_i^T is the tactile image, the o_i^A is the audio segment, the o_i^e is the robot end-effector pose, and a_i is the action. Then, we extract tactile and audio features (y_i^T, y_i^A) from the observations using our pre-trained encoders (shown in Sec. 3.2). These features and the corresponding robot end-effector pose serve as the input (y_i^T, y_i^A, o_i^e) to our model for generating the next action a_{i+1} . Given the varying scales of these inputs, we apply normalization such that the maximum distance for each input is unity in the dataset. During testing and experiment, for a given real-time observation \hat{o}_t , we compute the features $(\hat{y}_t^T, \hat{y}_t^A, \hat{o}_t^e)$. Then, we use these features to identify the data point in the dataset with the minimal aggregate distance, and subsequently execute the associated action.

3.4 Evaluation in Simulation

Since the current simulator is not able to generate high-quality tactile images and audio data, we need to do the RL fine-tuning directly on a physical robot. Hence, it is important to make sure that the latent policy is deployable to the physical robot environment. To validate the deployability of the learned latent policies on the physical robot, we first conduct evaluations within a simulated setting. We employ the Robosuite simulation framework [48], underpinned by the Mujoco Physics Engine [49], to simulate the real-world insertion task.

As depicted in Fig. 2, a table-top manipulation setup is established in the simulation to replicate the insertion task. The end-effector’s fingers are replaced with our custom fixture designed for the GelSight Mini. The object is fixed in proximity to the end-effector to prevent slippage during interactions. Given Mujoco’s constraint of supporting only convex objects, we construct a base with an insertion hole using four small cuboids. This setup allows us to execute the latent policy seamlessly. Details about latent policy and safety evaluations are shown in Sec. 4.2.

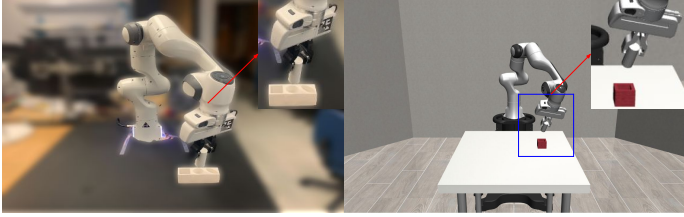


Figure 2: This figure shows our insertion task in both the physical robot environment and simulated environment, which are the same table-top settings containing a GelSight Mini fixture, a cylinder object, and an insertion base.

3.5 Learning Residual Policy through Online Reinforcement Fine-tuning

Although we have learned a latent policy from human demonstration, this latent policy might not guarantee task success when deployed on the physical robot. This is partially due to morphology differences between the human and robot end-effector, as well as the inaccurate tracking of the Aruco Marker. Therefore, we aim to further explore online reinforcement learning to enhance the latent policy. However, we cannot directly fine-tune the latent policy because it is learned through a non-parametric imitation learning manner. As a result, we propose to learn a residual policy that compensates for the embodiment gap issue through RL interactions (part (d) of Fig. 1). While the specifics of the implementation are still under consideration, we outline three potential methods that we believe hold promise. A detailed analysis of them is shown in Appendix. D.

3.5.1 Residual RL via Expert-Aligned Rewards

In recent research endeavors, a promising approach involves fine-tuning the latent policy through real-world interactions, aiming to align it with an expert policy [12, 19, 20]. These works employ optimal transport-based reinforcement learning to fine-tune the latent policy derived from expert data with expert-aligned rewards. Experimental results suggest that this technique can efficiently generate a robust policy, adaptable to analogous tasks across diverse environments. This is achieved with minimal training duration, even when the latent policy is derived from a small dataset.

3.5.2 Residual RL via Task-based Rewards

The task-based rewards represent a prominent methodology for refining the latent policy and facilitating the completion of insertion tasks. In related studies [9, 10], the authors introduce a tactile-based feedback insertion policy, utilizing reinforcement learning (RL) to model the insertion process as an episodic policy alternating between insertion attempts and pose corrections. With experiments evaluated on the physical robot, those papers show superior performance with RL using task-based rewards computed from tactile images.

3.5.3 Residual RL via Hybrid Expert-Aligned Rewards and Task-based Rewards

With the limitations of either expert-aligned rewards or task-based rewards are shown in Appendix. D, the hybrid method has been driven by several studies [17, 18]. In those studies, the authors employ both expert-aligned rewards and task-based rewards to refine the policy generated from human demonstration. Such a hybrid approach enhances the strengths of both methodologies, facilitating the extraction of task-based rewards to aid in task completion while concurrently upholding training safety standards. This potential approach is shown in part (d) of Fig. 1.

4 Experiments

In this section, we present the experiments with our MimicTouch framework.

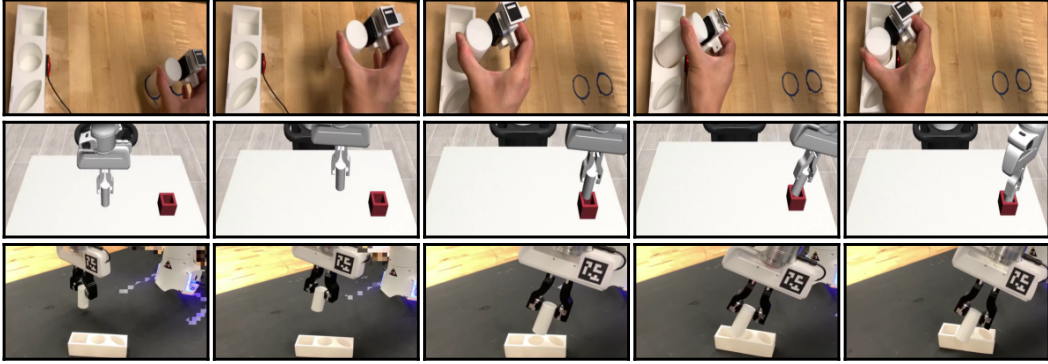


Figure 3: This figure shows the data collection process (first row), the latent policy shown in the simulated environment (second row), and the latent policy shown on the physical robot (third row).

4.1 Descriptions of Manipulation Tasks

To evaluate our framework, we set up two insertion tasks that require precise tactile feedback.

Long-horizon Insertion Task We 3D print three objects: a cylinder, a cuboid, and an elliptical cylinder with their hole base as shown in Fig. 2. We set up the task environments for both data collection in Sec. 3.1 and physical robot experiments (an example shown in Fig. 3). Starting from an initial position, the robot’s objective is to move to the top of the insertion base and complete the insertion task. This task is notably more challenging than standard insertion tasks. It requires the robot to emulate a blindfolded human who need to locate the insertion point and continuously adjust the object’s posture until finishing insertion. In contrast, traditional insertion tasks typically proceed without considering pose variations and consistently keep the object perpendicular to the table. For the data collection, we attempt to blindfold and insert the object with our tactile feedback to collect dataset to learn human’s tactile-guided control strategy. An example is shown in Fig. 3.

Another proposed unimplemented dense packing task is shown in Appendix. H.

4.2 Latent Policy Evaluation

In this section, we evaluate the latent policy learned from the human demonstration. Using the mean square error loss (MSE Loss, defined in Appendix. G), we can evaluate the difference between the generated actions and the ground truth actions.

Using the data collection system (Sec. 3.1), we collect 20 noisy-free data sequences with the trained encoder (Sec. 3.2) as the datasets to learn the latent policy. For policy evaluation, we gather another 10 data sequences with random noise, which helps to emulate the physical environments in the real world. Details of the noise added to the latent policy’s inputs are shown in Appendix. F.

To assess the efficacy and safety of the latent policy, we evaluate the actions generated by the latent policy with the data sequence in the emulated physical robot environment using the MSE Loss (reported in Table. 1) between the generated action sequence and the ground truth action sequence. We test three modes of generating the actions from the latent policy: 1). Use the recorded observation in the unseen data sequence to generate the next action, 2). Use the rollout robot state and the recorded sensor data to generate the next action, and 3). Use the noisy rollout robot states and noisy recorded sensor data to generate the next action (same method as in Appendix. F). From the table. 1, since all of those MSE Loss are similarly small, it shows that the latent policy can generate actions that are similar to the ground truth even with random noise. This indicates that the policy would **not** generate risky behaviors for the subsequent online RL fine-tuning on the physical robot.

Additionally, we visualize the retargeted action sequence and generated action sequence (mode 3) in the Robosuite simulated environment in Fig. 3, which shows that the rollout poses generated using VINN are close to the ground-truth retargeted pose.

States	Noise	MSE Loss
Desired States	No	0.14
Current States	No	0.21
Current States	Yes	0.26

Table 1: Average MSE Loss of 10 action sequences.

4.3 Ablation Study: Do Multi-Modal Tactile Feedback Improve the Performance?

In this section, we evaluate the performance of our multi-modal tactile embeddings.

Using the method outlined in 4.2, we evaluate the efficacy of our multi-modal tactile feedback by calculating the average MSE Loss of action sequences, generated from unseen data collected by humans with added random noise (mode 3). We evaluate our model with the following baselines:

- **MimicTouch w/o T & A:** MimicTouch without tactile or audio embeddings.
- **MimicTouch (T):** MimicTouch incorporating only tactile embeddings.
- **MimicTouch (A)** MimicTouch incorporating only audio embeddings.
- **MimicTouch (T + A, Ours):** MimicTouch incorporating both tactile and audio embeddings.

Models	MSE Loss
MimicTouch w/o T & A	0.62
MimicTouch (T)	0.38
MimicTouch (A)	0.48
MimicTouch (T + A, Ours)	0.26

From Table. 2, we report the MSE Loss between the generated actions and the ground truth actions. Without using both tactile images and audio signals, the MSE loss reaches 0.62, which is much higher than the others. In the case of using multi-modal tactile sensing, our approach outperforms the variants with a single modality.

Table 2: Average MSE Loss of 10 action sequences in the ablation study.

4.4 Physical Robot Experiment

In this section, we set up the physical robot experiment for both RL online fine-tuning and evaluation. The details about the robot setup and calibration are shown in Appendix. E

Latent Policy Firstly, we replay the retargeted motions and execute the latent policy on the physical robot. An example is shown in Fig. 3.

Currently, we only play the rollout actions generated from the latent policy in the emulated physical robot environment (shown in Sec. F) on the physical robot. In the future, we will collect real-time tactile images and audio signals as the input of the latent policy on the physical robot.

According to the example shown in Fig. 3, we can find that it is difficult to complete the task on the physical robot using the latent policy. This is partially due to morphology differences between the human and robot end-effector, as well as the inaccurate tracking of the Aruco Marker. Hence, we need to introduce online fine-tuning to mitigate this issue.

Baseline Models We propose to compare our model with the following baselines:

- **Tactile-RL [9]:** A baseline method uses pure RL policy generated from tactile images.
- **Active iSAM [10]:** A method estimates the contact line with tactile images, and uses the RL policy generated from the contact line.
- **MimicTouch w/o RL:** A variant of our model without RL fine-tuning
- **MimicTouch (T):** A variant of our model with only vision-based tactile feedback.

- **MimicTouch (A)**: A variant of our model with only audio-based tactile feedback.
- **MimicTouch (T+A, Ours)**

Notably, since our framework only uses human demonstration guided by tactile feedback, some other works that use visual feedback and teleoperation such as MULSA [6] are not considered.

Currently, we are conducting online RL fine-tuning and evaluating our approach in insertion tasks with those baseline models, and aim to show promising results by the time of this workshop presentation.

5 Conclusion & Future work

At present, this progressive project has achieved substantial advancements in the secure transference of human’s tactile-guided control strategies to physical robots, with evaluations affirming the efficacy of our proposed multi-modal tactile feedback in enhancing model performance. However, since this is an ongoing project, we acknowledge the limitations such as the latent policy directly generated from human demonstration might not achieve the task success on the physical robot. The next phase of this project will focus on integrating online residual reinforcement learning to overcome the identified limitations, and we intend to evaluate the overall performance of our proposed approach with other baseline methods. Additionally, we plan to conduct user studies to collect a diverse range of data from various individuals. Built upon our framework, people could explore other potential applications in learning a tactile-guided control strategy for different contact-rich challenging scenes without visual feedback.

References

- [1] B. Tang, M. A. Lin, I. Akinola, A. Handa, G. S. Sukhatme, F. Ramos, D. Fox, and Y. Narang. Industreal: Transferring contact-rich assembly tasks from simulation to reality. *arXiv preprint arXiv:2305.17110*, 2023.
- [2] Y. Narang, K. Storey, I. Akinola, M. Macklin, P. Reist, L. Wawrzyniak, Y. Guo, A. Moravanzky, G. State, M. Lu, A. Handa, and D. Fox. Factory: Fast contact for robotic assembly. *arXiv preprint arXiv:2205.03532*, 2022.
- [3] G. Schoettler, A. Nair, J. Luo, S. Bahl, J. A. Ojea, E. Solowjow, and S. Levine. Deep reinforcement learning for industrial insertion tasks with visual inputs and natural rewards. *arXiv preprint arXiv:1906.05841*, 2019.
- [4] G. Schoettler, A. Nair, J. A. Ojea, S. Levine, and E. Solowjow. Meta-reinforcement learning for robotic industrial insertion tasks. *arXiv preprint arXiv:2004.14404*, 2020.
- [5] G. Lengyel, G. Žalalytė, A. Pantelides, J. N. Ingram, J. Fiser, M. Lengyel, and D. M. Wolpert. Unimodal statistical learning produces multimodal object-like representations. *eLife*, 8:e43942, may 2019. ISSN 2050-084X. doi:10.7554/eLife.43942. URL <https://doi.org/10.7554/eLife.43942>.
- [6] H. Li, Y. Zhang, J. Zhu, S. Wang, M. A. Lee, H. Xu, E. Adelson, L. Fei-Fei, R. Gao, and J. Wu. See, hear, and feel: Smart sensory fusion for robotic manipulation. In *CoRL*, 2022.
- [7] M. A. Lee, Y. Zhu, K. Srinivasan, P. Shah, S. Savarese, L. Fei-Fei, A. Garg, and J. Bohg. Making sense of vision and touch: Self-supervised learning of multimodal representations for contact-rich tasks. In *2019 IEEE International Conference on Robotics and Automation (ICRA)*, 2019. URL <https://arxiv.org/abs/1810.10191>.
- [8] I. Guzey, B. Evans, S. Chintala, and L. Pinto. Dexterity from touch: Self-supervised pre-training of tactile representations with robotic play. *arXiv preprint arXiv:2303.12076*, 2023.
- [9] S. Dong, D. K. Jha, D. Romeres, S. Kim, D. Nikovski, and A. Rodriguez. Tactile-rl for insertion: Generalization to objects of unknown geometry. *arXiv preprint arXiv:2104.01167*, 2021.
- [10] S. Kim and A. Rodriguez. Active extrinsic contact sensing: Application to general peg-in-hole insertion. In *ICRA*, 2022.
- [11] Z.-H. Yin, B. Huang, Y. Qin, Q. Chen, and X. Wang. Rotating without seeing: Towards in-hand dexterity through touch. *arXiv preprint arXiv:2303.10880*, 2023.
- [12] K. Wang, Y. Zhao, and I. Sakuma. Learning robotic insertion tasks from human demonstration. *IEEE Robotics and Automation Letters*, 8(9):5815–5822, 2023. doi:10.1109/LRA.2023.3300238.
- [13] S. P. Arunachalam, I. Güzey, S. Chintala, and L. Pinto. Holo-dex: Teaching dexterity with immersive mixed reality. *arXiv preprint arXiv:2210.06463*, 2022.
- [14] A. Mandlekar, Y. Zhu, A. Garg, J. Booher, M. Spero, A. Tung, J. Gao, J. Emmons, A. Gupta, E. Orbay, S. Savarese, and L. Fei-Fei. Roboturk: A crowdsourcing platform for robotic skill learning through imitation. *arXiv preprint arXiv:1811.02790*, 2018.
- [15] C. Wang, L. Fan, J. Sun, R. Zhang, L. Fei-Fei, D. Xu, Y. Zhu, and A. Anandkumar. Mimicplay: Long-horizon imitation learning by watching human play. *arXiv preprint arXiv:2302.12422*, 2023.
- [16] K. Shaw, S. Bahl, and D. Pathak. Videodex: Learning dexterity from internet videos. *arXiv preprint arXiv:2212.04498*, 2022.

- [17] S. Bahl, A. Gupta, and D. Pathak. Human-to-robot imitation in the wild. *arXiv preprint arXiv:2207.09450*, 2022.
- [18] A. Kannan, K. Shaw, S. Bahl, P. Mannam, and D. Pathak. DEFT: Dexterous fine-tuning for real-world hand policies. In *7th Annual Conference on Robot Learning*, 2023. URL <https://openreview.net/forum?id=wH23nZpVTF6>.
- [19] S. Haldar, J. Pari, A. Rai, and L. Pinto. Teach a robot to fish: Versatile imitation from one minute of demonstrations. *arXiv preprint arXiv:2303.01497*, 2023.
- [20] S. Haldar, V. Mathur, D. Yarats, and L. Pinto. Watch and match: Supercharging imitation with regularized optimal transport. *arXiv preprint arXiv:2206.15469*, 2023.
- [21] W. Yuan, S. Dong, and E. H. Adelson. Gelsight: High-resolution robot tactile sensors for estimating geometry and force. *Sensors*, 17(12), 2017. ISSN 1424-8220. doi:10.3390/s17122762. URL <https://www.mdpi.com/1424-8220/17/12/2762>.
- [22] E. Donlon, S. Dong, M. Liu, J. Li, E. Adelson, and A. Rodriguez. Gelslim: A high-resolution, compact, robust, and calibrated tactile-sensing finger. *arXiv preprint arXiv:1803.00628*, 2018.
- [23] D. Ma, E. Donlon, S. Dong, and A. Rodriguez. Dense tactile force distribution estimation using gelslim and inverse fem. *arXiv preprint arXiv:1810.04621*, 2019.
- [24] S. Dong and A. Rodriguez. Tactile-based insertion for dense box-packing. *arXiv preprint arXiv:1909.05426*, 2019.
- [25] S. Suresh, Z. Si, J. G. Mangelson, W. Yuan, and M. Kaess. Shapemap 3-d: Efficient shape mapping through dense touch and vision. *arXiv preprint arXiv:2109.09884*, 2022.
- [26] E. J. Smith, R. Calandra, A. Romero, G. Gkioxari, D. Meger, J. Malik, and M. Drozdal. 3d shape reconstruction from vision and touch. *arXiv preprint arXiv:2007.03778*, 2020.
- [27] E. J. Smith, D. Meger, L. Pineda, R. Calandra, J. Malik, A. Romero, and M. Drozdal. Active 3d shape reconstruction from vision and touch. *arXiv preprint arXiv:2107.09584*, 2021.
- [28] R. Calandra, A. Owens, D. Jayaraman, J. Lin, W. Yuan, J. Malik, E. H. Adelson, and S. Levine. More than a feeling: Learning to grasp and regrasp using vision and touch. *IEEE Robotics and Automation Letters*, 3(4):3300–3307, oct 2018. doi:10.1109/lra.2018.2852779. URL <https://doi.org/10.1109/lra.2018.2852779>.
- [29] L. Pinto, D. Gandhi, Y. Han, Y.-L. Park, and A. Gupta. The curious robot: Learning visual representations via physical interactions. *arXiv preprint arXiv:1604.01360*, 2016.
- [30] R. Calandra, A. Owens, M. Upadhyaya, W. Yuan, J. Lin, E. H. Adelson, and S. Levine. The feeling of success: Does touch sensing help predict grasp outcomes? *arXiv preprint arXiv:1710.05512*, 2017.
- [31] Y. Han, K. Yu, R. Batra, N. Boyd, C. Mehta, T. Zhao, Y. She, S. Hutchinson, and Y. Zhao. Learning generalizable vision-tactile robotic grasping strategy for deformable objects via transformer. *arXiv preprint arXiv:2112.06374*, 2023.
- [32] A. Thankaraj and L. Pinto. That sounds right: Auditory self-supervision for dynamic robot manipulation. *arXiv preprint arXiv:2210.01116*, 2022.
- [33] J. Sinapov, M. Wiemer, and A. Stoytchev. Interactive learning of the acoustic properties of household objects. In *2009 IEEE International Conference on Robotics and Automation*, pages 2518–2524, 2009. doi:10.1109/ROBOT.2009.5152802.
- [34] J. Christie and N. Kottege. Acoustics based terrain classification for legged robots. In *2016 IEEE International Conference on Robotics and Automation (ICRA)*, pages 3596–3603, 2016. doi:10.1109/ICRA.2016.7487543.

- [35] C. Matl, Y. Narang, D. Fox, R. Bajcsy, and F. Ramos. Stressd: Sim-to-real from sound for stochastic dynamics. *arXiv preprint arXiv:2011.03136*, 2020.
- [36] D. Gandhi, A. Gupta, and L. Pinto. Swoosh! rattle! thump! – actions that sound. *arXiv preprint arXiv:2007.01851*, 2020.
- [37] A. Sawhney, S. Lee, K. Zhang, M. Veloso, and O. Kroemer. Playing with food: Learning food item representations through interactive exploration. *arXiv preprint arXiv:2101.02252*, 2021.
- [38] Y. Qin, Y.-H. Wu, S. Liu, H. Jiang, R. Yang, Y. Fu, and X. Wang. Dexmv: Imitation learning for dexterous manipulation from human videos. *arXiv preprint arXiv:2108.05877*, 2022.
- [39] J. Ho and S. Ermon. Generative adversarial imitation learning. *arXiv preprint arXiv:1606.03476*, 2016.
- [40] M. Xie, A. Handa, S. Tyree, D. Fox, H. Ravichandar, N. D. Ratliff, and K. V. Wyk. Neural geometric fabrics: Efficiently learning high-dimensional policies from demonstration. In K. Liu, D. Kulic, and J. Ichnowski, editors, *Proceedings of The 6th Conference on Robot Learning*, volume 205 of *Proceedings of Machine Learning Research*, pages 1355–1367. PMLR, 14–18 Dec 2023.
- [41] Y. Han, M. Xie, Y. Zhao, and H. Ravichandar. On the utility of koopman operator theory in learning dexterous manipulation skills. *arXiv preprint arXiv:2303.13446*, 2023.
- [42] Y. Huang, L. Rozo, J. Silvério, and D. G. Caldwell. Non-parametric imitation learning of robot motor skills. In *2019 International Conference on Robotics and Automation (ICRA)*, pages 5266–5272, 2019. doi:10.1109/ICRA.2019.8794267.
- [43] M. Vaandrager, R. Babuška, L. Buşoniu, and G. A. Lopes. Imitation learning with non-parametric regression. In *Proceedings of 2012 IEEE International Conference on Automation, Quality and Testing, Robotics*, pages 91–96, 2012. doi:10.1109/AQTR.2012.6237681.
- [44] J. Pari, N. M. Shafiqullah, S. P. Arunachalam, and L. Pinto. The surprising effectiveness of representation learning for visual imitation. *arXiv preprint arXiv:2112.01511*, 2021.
- [45] Gelsight mini. <https://www.gelsight.com/gelsightmini/>.
- [46] J.-B. Grill, F. Strub, F. Altché, C. Tallec, P. H. Richemond, E. Buchatskaya, C. Doersch, B. A. Pires, Z. D. Guo, M. G. Azar, B. Piot, K. Kavukcuoglu, R. Munos, and M. Valko. Bootstrap your own latent: A new approach to self-supervised learning. *arXiv preprint arXiv:2006.07733*, 2020.
- [47] D. Niizumi, D. Takeuchi, Y. Ohishi, N. Harada, and K. Kashino. Byol for audio: Self-supervised learning for general-purpose audio representation. *arXiv preprint arXiv:2103.06695*, 2021.
- [48] Y. Zhu, J. Wong, A. Mandlekar, R. Martín-Martín, A. Joshi, S. Nasiriany, and Y. Zhu. robosuite: A modular simulation framework and benchmark for robot learning. *arXiv preprint arXiv:2009.12293*, 2022.
- [49] E. Todorov, T. Erez, and Y. Tassa. Mujoco: A physics engine for model-based control. In *2012 IEEE/RSJ International Conference on Intelligent Robots and Systems*, pages 5026–5033, 2012. doi:10.1109/IROS.2012.6386109.
- [50] S. Garrido-Jurado, R. Muñoz-Salinas, F. J. Madrid-Cuevas, and M. J. Marín-Jiménez. Automatic generation and detection of highly reliable fiducial markers under occlusion. *Pattern Recognit.*, 47:2280–2292, 2014. URL <https://api.semanticscholar.org/CorpusID:12519167>.

- [51] M. S. Kanishke Gamagedara, Jean Gressmann. aruco-markers. <https://github.com/fdcl-gwu/aruco-markers.git>, 2018.
- [52] K. He, X. Zhang, S. Ren, and J. Sun. Deep residual learning for image recognition. *arXiv preprint arXiv:1512.03385*, 2015.

Appendices

A Fingertips Pose Tracking

To track the human fingertip motions, we put an Aruco marker [50] on our custom fixture to track human fingertip movements. Positioned in a tabletop view, the RealSense camera captures the Aruco marker’s pose. Using an open-source library [51], the marker’s 6D pose was tracked at 60Hz. These human fingertip poses are subsequently mapped to the robot end-effector’s pose, serving as vital input for the imitation learning process after retargeting and post-processing (shown in Sec. 3.3).

B Representation Learning

BYOL BYOL [46] generates two augmented views, $v \triangleq t(x)$ and $v' \triangleq t'(x)$, from a given x by applying image augmentations $t \sim \mathcal{T}$ and $t' \sim \mathcal{T}'$ respectively, where \mathcal{T} and \mathcal{T}' represent distinct augmentation distributions. The architecture of BYOL comprises a primary encoder f_θ and a target encoder f_ξ , where the latter being an exponential moving average of the former. Given the augmented views v and v' , they are processed to yield representations y and y' . These representations are subsequently transformed by projectors g_θ and g_ξ to produce higher-dimensional vectors z and z' . The primary encoder and its associated projector are designed to predict the output from the target projector, resulting in $q_\theta(z_\theta)$ and $sg(z'_\xi)$. The model’s output consists of l_2 -normalized versions of these predictions, which are trained using a similarity loss function. Post-training, the encoder f_θ is utilized for feature extraction from observations.

To utilize BYOL in tactile images, we scale the tactile image up to 256x256 to work with standard image encoders. We use the ResNet [52] architecture, also starting with pre-trained weights. Unlike SSL techniques in visual images, we only apply the Gaussian blur and small center-resized crop augmentations, since other augmentations such as color jitter and grayscale would violate the assumption that augmentations do not change the tactile signal significantly. For each input, the trained model will generate a 1×2048 representation vector.

Audio Representation Learning BYOL-A [47] is an extended version of BYOL to audio representation learning, processing log-scaled mel-spectrograms through a specialized augmentation module. To utilize BYOL-A in our audio data, we down-sampled signals from 44.1kHz to 16kHz, with a window size of 64 ms, a hop size of 10 ms, and mel-spaced frequency bins $F = 64$ in the range 60–7,800 Hz. Then, the Pre-Normalization step stabilizes the input audio for subsequent augmentations. Once normalized, the Mixup step introduces contrasts in the audio’s background, defined by the log-mixup-exp formula:

$$\tilde{x}_i = \log((1 - \lambda) \exp(x_i) + \lambda \exp(x_k))$$

where x_k is a mixing counterpart and λ is a ratio from a uniform distribution. The next one is the RRC block, an augmentation technique, that captures content details and emulates pitch shifts and time stretches. For each input, the trained model will generate a 1×2048 representation vector.

C Post Processing

Given the inherent noise and occasional outliers in the poses obtained from the RealSense and Aruco markers, it is imperative to implement post-processing techniques to ensure the quality and smoothness of the trajectories. For each pose sequence, outliers are detected by sorting the values of each delta transformation. The Interquartile Range (IQR) method is employed to establish the upper and lower bounds, which are then used to identify outliers. The IQR is defined as: $IQR = Q_3 - Q_1$ where Q_3 and Q_1 are the third and first quartiles, respectively. Outliers are replaced using a median filter with a window size of 3. To enhance the temporal consistency of the estimated hand and object

pose, a digital low-pass filter is applied to eliminate high-frequency noise. Specifically, the filter has a sampling frequency of 5HZ and a cutoff frequency of 2HZ. The low-pass filter can be represented as: $H(f) = \frac{1}{1+(\frac{f}{f_c})^2}$ where f is the sampling frequency and f_c is the cutoff frequency.

D Analysis of RL Fine-tuning

Residual RL via Expert-Aligned Rewards Such algorithms demonstrate the capacity to efficiently learn policies that are generalizable across similar tasks in diverse environments. A salient feature of this approach is its emphasis on aligning the robotic policy with that of experts, ensuring the assimilation of safety-centric policies from these experts. This safety alignment is important, especially when dealing with out-of-domain datasets. However, the efficacy of these methods has been primarily validated using the in-domain training data, which only encompasses configuration gaps from visual imagery. Their applicability to out-of-domain datasets, especially those with embodiment gap remains unexplored. Due to the embodiment gap, the expert policies, which are retargeted from human demonstrations, often prove incompatible with direct robotic applications. Consequently, the endeavor to align robotic policies with potentially non-transferable datasets may not effectively address the embodiment gap issue.

Residual RL via Task-based Rewards Utilizing task-based rewards are helpful in completing insertion tasks. Compared to the expert-aligned reward. It may better address the embodiment gap issue. However, this method has not been used in fine-tuning a pre-trained latent policy learned from human demonstrations. Besides, from the paper [12], we see numerous constraints were introduced to ensure training safety. In such intricate tasks in Sec. 4.1, we encourage the RL exploration while incorporating other safety constraints presents a great challenge. Furthermore, task-based rewards are ideally sparse in nature. In our task, the robots need to constantly adjust their pose, which is a very continuous motion. As a result, using sparse rewards might exacerbate training complexities and reduce overall training efficiency.

Residual RL via Hybrid Expert-Aligned Rewards and Task-based Rewards The hybrid strategy has been proven that it can utilize both advantages of different rewards with human visual feedback. It can not only ensure safe training and fast fine-tuning but also mitigate the embodiment gap. Thus, we hope that this method can also play a good role in fine-tuning the human demonstration with tactile feedback.

E Setup

Robot Setup All experiments are conducted on a Franka Emika Panda Arm. An inverse kinematics solver is used to map the 6-DoF Cartesian space displacement commands into the 7-DoF joint actions. For each task, Cartesian space displacement commands are generated at a policy frequency of 5 Hz, subsequently mapped by the low-level control loop to force and torque inputs in the robot’s joint space at 200 Hz.

Calibration Given that our data collection and final experiments occur in disparate scenarios, it’s crucial to align our human-centric data collection system with the physical robot system. Initially, we record the distance between the object (starting point) and the base (ending point) within the data collection system and replicate this setup in the robot environment. Following this, six equidistant positions between the starting and ending points are identified within both systems. The object is gripped at these predetermined positions using both hands and the robot’s end-effector, allowing us to capture the corresponding poses. In this calibration process, the hand poses, denoted as the “Eye” in the calibration function, are referenced to the camera frame, while the end-effector poses, represented as the “Hand” in the calibration system, are referenced to the robot frame. Conclusively, we employ the `calibrateHandEye` function from OpenCV, using the six captured poses, to calibrate these two frames (camera frame and robot frame).

F Emulate the Physical Robot Environment

Add Random Noise To emulate the physical robot environment, we introduce random noise to those 10 unseen data sequences. The robot state space input undergoes a random position noise within the range $[-3\text{cm}, +3\text{cm}]$ for each axis. Gaussian noise, denoted as $\mathcal{N}(0, \sigma)$, is added to both the tactile image and audio signal. In this notation, $\mathcal{N}(0, \sigma)$ signifies a Gaussian distribution with a mean of 0 and a standard deviation of σ . For tactile images, the noise affects pixel values in the range $[0, 255]$, while for audio data, it impacts signal values in the range $[0, 1]$. Given their distinct ranges, we apply Gaussian noise with standard deviations of $\sigma = 100$ for tactile images and $\sigma = 0.4$ for audio data.

Generate Action Sequence To evaluate the latent policy with those unseen data sequences with noises, we follow these steps: 1). For the first initial pose, we use the collected pose, tactile image, and audio data, all subjected to noise. 2). For subsequent poses, our VINN model is employed to generate a new pose utilizing the pose and sensor data from the preceding state. Then, we add noises on the newly synthesized pose and the multi-modal tactile data derived from the original unseen action sequence corresponding to the current time step. The synthesized pose and tactile data with noises will be used for generating the next pose. 3). After obtaining a trained sequence with the same length as the original unseen data sequence, we finish the generation of action sequences.

G MSE Loss

For calculating the MSE Loss between two action sequences, we need to normalize the actions' translation vectors and rotation vectors since they have different scales. Then, we calculate the average MSE Loss between each action of these two action sequences. The formula is shown as:

$$\text{MSE} = \frac{1}{n} \sum_{i=1}^n (y_i - \hat{y}_i)^2$$

Where: y_i represents the ground truth action, \hat{y}_i represents the generated action, and n is the number of all action steps.

H Dense Packing

The objective of this task is to accurately insert an object into a constrained space within a nearly saturated box. To accomplish this goal, the robot is required to initially relocate the object from its starting position to a point above the box, subsequently navigate around obstacles, identify the available space within the box, and ultimately execute the insertion accurately. We conduct two variations of dense packing: one employing 3D printed objects, facilitating a more controlled examination of each modality's role in this task, and another utilizing diverse real-world objects. An example is shown in Fig. 4. We will implement this task after evaluating the long-horizon insertion task.



Figure 4: An example for the dense packing task.